# Structural stability and energy-gap modulation through atomic protrusion in freestanding bilayer silicene

Yuki Sakai and Atsushi Oshiyama

*Department of Applied Physics, University of Tokyo, 7-3-1, Hongo, Bunkyo-ku, Tokyo 113-8656, Japan*
(Received 25 December 2014; revised manuscript received 23 April 2015; published 11 May 2015)

We report on first-principles total-energy and phonon calculations that clarify structural stability and electronic properties of freestanding bilayer silicene. By extensive structural exploration, we reach all the stable structures reported before and find four additional dynamically stable structures, including the structure with the largest cohesive energy. We find that atomic protrusion from the layer is the principal relaxation pattern which stabilizes bilayer silicene and determines the lateral periodicity. The hybrid-functional calculation shows that the most stable bilayer silicene is a semiconductor with the energy gap of 1.3 eV.

Bilayer graphene provides new aspects of graphene physics such as the band gap opening [1–4] and moiré-pattern-induced electron localization [5,6]. The interlayer interaction is obviously weaker than the intralayer interaction but decisive to modulate the electron states due to its symmetry breaking. Similar intriguing behavior with the extension related to the spin degrees of freedom is expected [7–9] for layered Si (silicene), which has been grown experimentally with a form of a monolayer [10–17] and of a few layers [18–22] mainly on Ag substrates. One of the most important characteristics which discriminate silicene from graphene is the buckling of two sublattices caused by the preference of Si for $sp^3$ hybridization. In fact, first-principles calculations within the local density approximation [23,24] have clarified that a planar Si monolayer is unstable to the buckling, and that the resultant freestanding monolayer silicene with a buckling of 0.44 Å has the Dirac cone at the Fermi level, $E_F$. This buckling brings about a complex but rich variation in structure and electronic properties in bilayer silicene, which we address in this Rapid Communication.

Several theoretical investigations have been performed on freestanding bilayer silicene [25–31]. A flat bilayer structure with perfect overlapping stacking ($AA$ stacking) has been predicted based on a molecular dynamics simulation [25]. A corrugated $2 \times 2$ (rectangular supercell) reconstructed structure different from the well known $\pi$-bonded chain structure of the Si(111) surface [32] has been also found [26]. Recently, freestanding bilayer silicene has been found to have several local minima in total energy as a function of the lateral lattice parameter, suggesting its wealth of the structural diversity [27]. A possible structural phase transition under the lateral strain has been also discussed [28]. To validate such theoretical predictions, however, a systematic exploration of stable structures with their thermal excitation spectra (phonons), which is lacking in the past, is imperative. Further, clarification of correlation between the structural diversity and its role in electronic properties is highly demanded.

We here perform systematic first-principles total-energy and phonon calculations for freestanding bilayer silicene with various lateral periodicities and atomic densities. By extensive geometry optimization followed by the phonon calculations, we unequivocally identify ten dynamically stable structures with distinct atomic configurations, symmetries, and

periodicities. We clarify that the ten structures include all six structures reported in the past. Four additional structures are also found and are more stable than the previously reported ones. We find that the more stable structures have a single prominent structural characteristic, i.e., the protrusion of the Si atom. We also find that there is an energetically optimum lateral periodicity for the protruded structure, i.e., $\sqrt{3} \times \sqrt{3}$ or $2 \times 2$, depending on the stacking of the two Si layers. We further clarify that the stable freestanding bilayer silicene is a semiconductor in which the energy gap is sensitive to the detailed protruded structure.

We use the pseudopotential-plane-wave method [33,34] based on density-functional theory [35,36]. We adopt the exchange-correlation functionals developed by Perdew, Burke, and Ernzerhof (PBE) [37]. We crosscheck the electronic properties by using the Heyd-Scuseria-Ernzerhof (HSE) hybrid functional [38,39]. Phonon dispersion relations are calculated based on density-functional perturbation theory [40–42]. Computational details are described in the Supplemental Material [43].

In our calculations, we have considered $1 \times 1$, $2 \times 2$, $\sqrt{3} \times \sqrt{3}$, and $\sqrt{7} \times \sqrt{7}$ lateral periodicities with respect to the monolayer periodicity and performed total-energy optimization. Freestanding monolayer silicene is intrinsically buckled so that the stacking of two Si monolayers is of rich variety: the buckling of two layers may be in-phase, out-of-phase, or planar both in the $AA$ stacking and in the $AB$ stacking (Bernal stacking named in graphite); further, the stacking is not restricted to $AA$ or $AB$ but could be orthorhombic (OR) in general. We have then noticed that there are 16 distinct stacking configurations [43]. For each stacking configuration, we have adopted a certain lateral lattice parameter and fully optimized atomic geometries, and then repeated the calculations with varying the lattice parameter. We have also examined the possibility of a unit-cell distortion. By such extensive exploration, we have obtained 24 distinct total-energy minimized geometries for the $1 \times 1$, $2 \times 2$, and $\sqrt{3} \times \sqrt{3}$ periodicities. We have then calculated the phonon spectra for thus obtained total-energy minimized structures. Surprisingly, 14 of the 24 total-energy minimized structures are clarified as being unstable with imaginary phonon frequencies, although their interlayer binding energies are positive. We have then eventually reached four $1 \times 1$, four $2 \times 2$, and
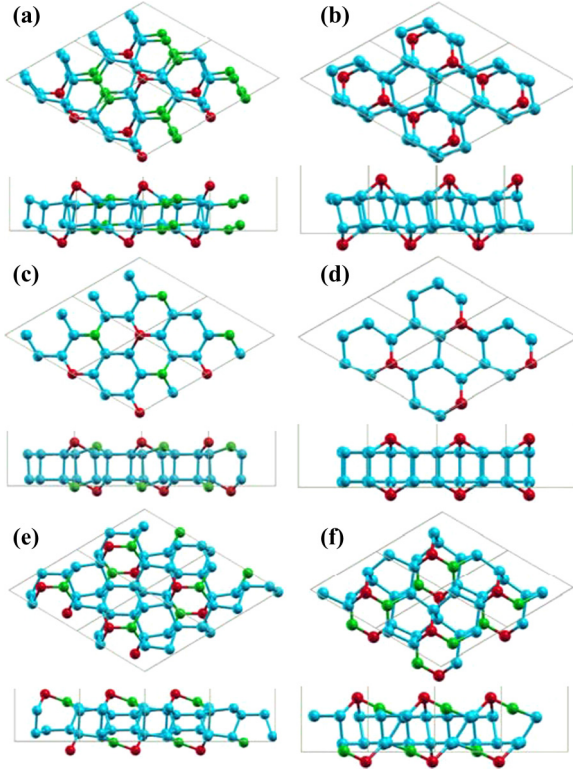
FIG. 1. (Color online) Total-energy minimized structures of $\sqrt{3} \times \sqrt{3}$ and $2 \times 2$ freestanding bilayer silicene: (a) slide-$2 \times 2$, (b) slide-$\sqrt{3} \times \sqrt{3}$, (c) $AA$-$2 \times 2$, (d) $AA$-$\sqrt{3} \times \sqrt{3}$, (e) hex-OR-$2 \times 2$, and (f) OR-$\sqrt{3} \times \sqrt{3}$ structures. Unit cells are represented by silver lines. Blue, red, and green spheres represent fourfold-coordinated, highly protruded, and moderately protruded silicon atoms, respectively. The angle between two lattice vectors is slightly changed from $120°$ in the slide-$2 \times 2$, slide-$\sqrt{3} \times \sqrt{3}$, hex-OR-$2 \times 2$, and OR-$\sqrt{3} \times \sqrt{3}$ cases. The XCrySDen program is used for visualization of the atomic structures [44].

two $\sqrt{3} \times \sqrt{3}$ dynamically stable structures. Details of our structural exploration are described in the Supplemental Material [43].

The five dynamically stable structures obtained in the present study shown in Fig. S4 of the Supplemental Material [43] and Fig. 1(a), which are named $AA$-$1 \times 1$, $AB$-$1 \times 1$, slide-$1 \times 1$, OR-$1 \times 1$, and slide-$2 \times 2$, are presumably identical to the structures which have been reported previously [26–30]. The $AA$-$1 \times 1$ structure is similar to the $AA$-stacking bilayer graphene, but the interlayer distance is significantly small (2.411 Å), resulting in the fourfold coordination of all the Si atoms. The $AB$-$1 \times 1$ structure is similar to an atomic slab in the diamond structure, inferring the existence of threefold-coordinated Si. The slide-$1 \times 1$ structure also shows threefold- and fourfold-coordinated atoms, although the interlayer distance becomes shorter compared to the $AB$-$1 \times 1$. The OR-$1 \times 1$ structure is obtained by relaxing the lateral and in-plane bond angles of $AA$-$1 \times 1$ structure. The $AA$-$1 \times 1$, $AB$-$1 \times 1$, slide-$1 \times 1$, OR-$1 \times 1$, and slide-$2 \times 2$ structures are presumably identical to the $1AA$, $1AB$, and slide-$2AA$ structures in Ref. [27], the Si-$Cmme$ structure in Ref. [29], and the phase II structure obtained in Ref. [28],

TABLE I. Calculated total energies (in meV/atom) of various stacking geometries ($AA$, slide, OR, and $AB$) and lateral periodicities ($1 \times 1$, $\sqrt{3} \times \sqrt{3}$, $2 \times 2$, and $\sqrt{7} \times \sqrt{7}$) of freestanding bilayer silicene. The total energies are compared to that of freestanding monolayer silicene. We do not find a distinct $AB$-stacking structure for the $\sqrt{3} \times \sqrt{3}$ and $2 \times 2$ periodicities.

| Stacking | Periodicity | | | |
|---|---|---|---|---|
| | $1 \times 1$ | $\sqrt{3} \times \sqrt{3}$ | $2 \times 2$ | $\sqrt{7} \times \sqrt{7}$ |
| $AA$ | −183 | −230 | −220 | −217 |
| Slide | −149 | −234 | −255 | −223 |
| OR | −201 | −252 | −261 (hex) −251 (rect) | −219 |
| $AB$ | −130 | | | |

respectively. We have also obtained the structure proposed in Ref. [26], here denoted by rect-OR-$2 \times 2$ [Fig. S4(e)], by using a rectangular $2 \times 2$ supercell. The slide-$2 \times 2$ and the rect-OR-$2 \times 2$ structures exhibit peculiar structural characteristics: two Si atoms in each unit cell protrude prominently, causing the local tetrahedral geometry. It is noteworthy that this protrusion renders those two structures lower in energy than the other 4 structures (see below).

In the $2 \times 2$ periodicity, we have found two additional structures, named $AA$-$2 \times 2$ [Fig. 1(c)] and hex-OR-$2 \times 2$ [Fig. 1(e)]. The latter is the lowest in energy among the structures ever reported (see below). The $AA$-$2 \times 2$ structure shows common characteristics to the slide-$2 \times 2$ structure [Fig. 1(a)], but the details are different. The $AA$-$2 \times 2$ structure possesses almost complete $AA$ stacking whereas the slight dislodgment is observed in the slide-$2 \times 2$. In the $AA$-$2 \times 2$, two silicon atoms in each unit cell are highly protruded [red spheres in Fig. 1(c)] whereas another two atoms are moderately protruded (green spheres). In the hex-OR-$2 \times 2$ structure, on the other hand, red and green protruded Si atoms in Fig. 1(e) form dimers. The hex-OR-$2 \times 2$ structure is similar to the rect-OR-$2 \times 2$ structure although the supercell is not rectangular but hexagonal. The four $2 \times 2$ structures, including the additional two structures, are dynamically stable, as is evidenced from their calculated phonon spectra shown in Figs. 2(a), 2(c), and 2(e), and in Fig. S4(j).

We have further explored dynamically stable structures with different lateral periodicity. Focusing on the dynamically stable stacking configurations in the $2 \times 2$ periodicity shown in Figs. 1(a), 1(c), and 1(e), we have examined the $\sqrt{3} \times \sqrt{3}$ lateral periodicity with those stackings. We have found that the $AA$- and OR-$\sqrt{3} \times \sqrt{3}$ structures [Figs. 1(d) and 1(f)] are also dynamically stable whereas the slide-$\sqrt{3} \times \sqrt{3}$ structure [Fig. 1(b)] is unstable, as is evidenced in our phonon dispersion relations in Figs. 2(b), 2(d), and 2(f). To our knowledge, the $AA$- and the OR-$\sqrt{3} \times \sqrt{3}$ structures found here have not been reported in the past.

The calculated total energies of freestanding bilayer silicene with various stackings and periodicities are listed in Table I. The hex-OR-$2 \times 2$ structure found here has the lowest energy, and the slide-$2 \times 2$ follows with the total-energy increase of 6 meV/atom. The OR-$\sqrt{3} \times \sqrt{3}$ and rect-OR-$2 \times 2$ structures are also close in energy (+9 and +10 meV/atom from the
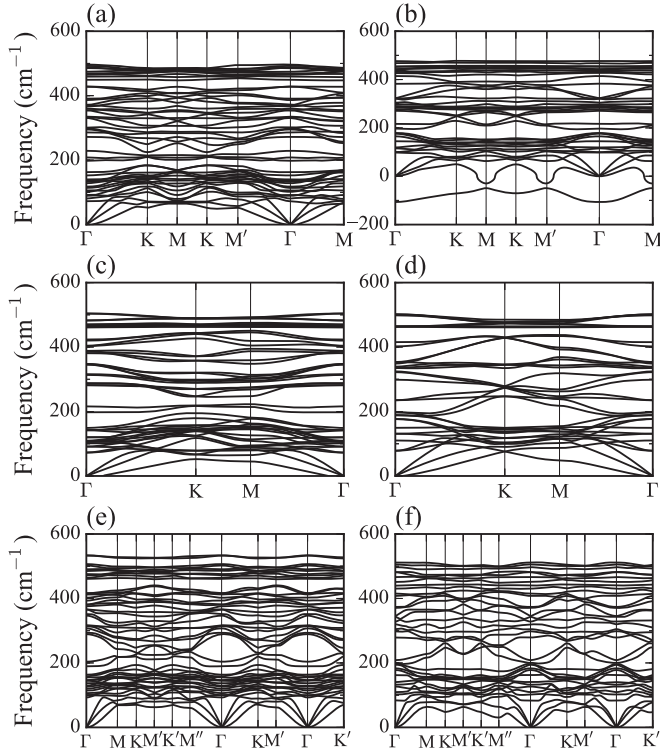
FIG. 2. Phonon dispersion relations of (a) slide-$2 \times 2$, (b) slide-$\sqrt{3} \times \sqrt{3}$, (c) $AA$-$2 \times 2$, (d) $AA$-$\sqrt{3} \times \sqrt{3}$, (e) hex-OR-$2 \times 2$, and (f) OR-$\sqrt{3} \times \sqrt{3}$ structures (in the same order as Fig. 1). Phonon dispersions crossing several $M$ points, $M(0.5,0)$, $M'(0,0.5)$, and $M''(-0.5,0.5)$, in units of reciprocal lattice vector, which are inequivalent to each other in the low-symmetry cases, are plotted. The negative values in (b) mean imaginary phonon frequencies, indicating that the structure is dynamically unstable. Imaginary frequency branches (acoustic vibrational modes along the direction perpendicular to the layers) appear around the $\Gamma$ point in other cases due to the interpolation errors. We have confirmed that these imaginary frequencies become real when we directly compute the phonon frequency at specific **q** points with sufficient vacuum space (16 Å) of the supercell and cutoff energy (60 Ry).



FIG. 3. (Color online) Top view of OR-$\sqrt{7} \times \sqrt{7}$ structure. Red and green spheres are highly protruded and moderately protruded Si atoms as in Figs. 1(e) and 1(f). Black spheres represent additionally protruded Si atoms.

lowest energy, respectively). The $AA$-$\sqrt{3} \times \sqrt{3}$ and $AA$-$2 \times 2$ are in the second lowest energy group ($+31$ and $+41$ meV/atom, respectively). The OR-, $AA$-, slide-, $AB$-$1 \times 1$ structures have relatively high energy ($+60$, $+78$, $+112$, and $+131$ meV/atom, respectively) compared to the $\sqrt{3} \times \sqrt{3}$ and $2 \times 2$ structures. We have also calculated the total energy of another structure named honeycomb dumbbell silicene [45], constructed from a $3 \times 3$ monolayer silicene. This dumbbell structure is outside our configurational phase space for the structural search, although it has higher total energy than the value of the hex-OR-$2 \times 2$ structure by 206 meV/atom ($\sqrt{3} \times \sqrt{3}$ periodicity) or 60 meV/atom ($2 \times 2$ periodicity).

Our systematic total-energy and phonon calculations have clarified the rich structural variety of bilayer silicene. At the same time, it has become clear that stable bilayer silicene is accompanied with a characteristic relaxation, i.e., the atomic protrusion. The $\sqrt{3} \times \sqrt{3}$ structures and their structural analogs with the $2 \times 2$ periodicity have common stacking configurations and protruded structures but different total energies.
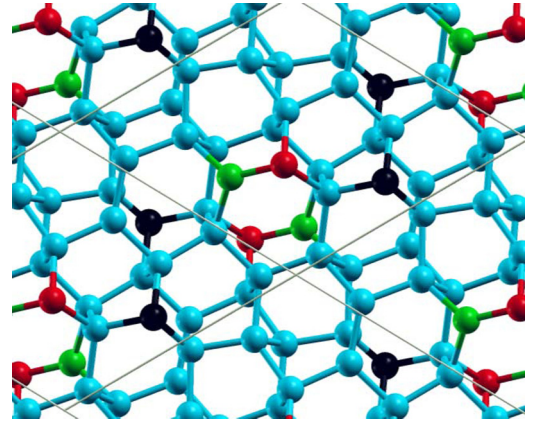
This implies the existence of an optimum periodicity for the protruded structure for each stacking configuration. In order to clarify this point, we have performed total energy calculations for the $\sqrt{7} \times \sqrt{7}$ structures having the characteristic protruded pattern for the three stacking geometries ($AA$, slide, and OR). The total energies of the fully optimized $\sqrt{7} \times \sqrt{7}$ structures are shown in Table I. They are all higher than the corresponding total energies of the $2 \times 2$-periodicity cases. The total energies of the slide and OR stacking geometries become minimum with the $2 \times 2$ periodicity, whereas the total energy of the $AA$ stacking is minimum at the $\sqrt{3} \times \sqrt{3}$ periodicity. We have now unveiled that the atomic protrusion is the principal relaxation pattern which stabilizes the bilayer silicene and induces a particular lateral periodicity.

Figure 3 shows the top view of the OR-$\sqrt{7} \times \sqrt{7}$ structure obtained here. Red and green spheres represent dimerized protrusion which is common to other periodicities. We now find that extra Si protrusions (black spheres) are induced in the $\sqrt{7} \times \sqrt{7}$ periodicity which are absent in the shorter periodicity. The protrusion generates the local tetrahedral geometry which is favorable for Si but at the same time induces stress energy around. The structure with the $\sqrt{7} \times \sqrt{7}$ periodicity indicates that the incomplete protrusion is energetically unfavorable. Similarly, the $AA$- and slide-$\sqrt{7} \times \sqrt{7}$ structures also show the extra protrusions. Such extra protrusions are also found in the $AA$-$2 \times 2$ structure where four of 16 Si atoms are protruded in each cell while the $AA$-$\sqrt{3} \times \sqrt{3}$ has one protruded atom in six Si atoms [Figs. 1(c) and 1(d)]. This excess protrusion is also observed in the highest-energy $AB$-$1 \times 1$ structure where half of Si atoms are protruded. The hex-OR-$2 \times 2$ structure which we have found has the lowest energy and is free from such extra protrusion.

Figure 4 shows the PBE band structures of the four most stable bilayer silicenes, slide-$2 \times 2$, $AA$-$\sqrt{3} \times \sqrt{3}$, OR-$\sqrt{3} \times \sqrt{3}$, and hex-OR-$2 \times 2$. The total energy differences of these four structures are within the range of 31 meV/atom, indicating that they are stable at room temperature. The slide-$2 \times 2$, $AA$-$\sqrt{3} \times \sqrt{3}$, and OR-$\sqrt{3} \times \sqrt{3}$ structures are narrow-gap semiconductors with indirect band gaps of 0.07 ($K$-$M$ line $\to \Gamma$), 0.06 ($M \to \Gamma$), and 0.02 eV ($M \to M''$),
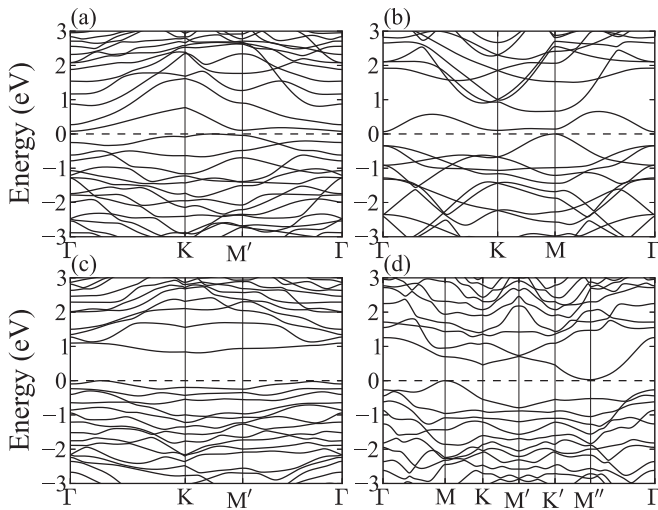
FIG. 4. PBE band structures of dynamically stable (a) slide-$2 \times 2$, (b) $AA$-$\sqrt{3} \times \sqrt{3}$, (c) hex-OR-$2 \times 2$, and (d) OR-$\sqrt{3} \times \sqrt{3}$ structures. The horizontal dashed line indicates the valence-band top. The path is chosen so that valence-band top and conduction-band bottom can be seen in the plot.
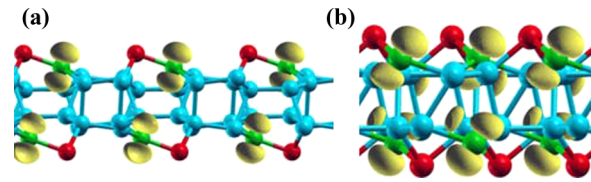


FIG. 5. (Color online) Conduction band bottom Kohn-Sham wave functions of (a) hex-OR-$2 \times 2$ and (b) OR-$\sqrt{3} \times \sqrt{3}$ structures. The yellow isosurfaces represent 1/3 of the maximum amplitude.

respectively. The band gaps of the three structures become approximately 0.37, 0.34, and 0.40 eV, respectively, when we use the hybrid HSE functional. Interestingly, the indirect band gap ($\Gamma$-$K$ line $\to$ $K$-$M$ line) of the most stable hex-OR-$2 \times 2$ structure is 0.8 eV (about 1.3 eV in the HSE calculation), considerably wide compared to other structures.

The hex-OR-$2 \times 2$ and OR-$\sqrt{3} \times \sqrt{3}$ structures have common protrusion but remarkably different band gaps. The conduction-band bottom state is more dispersive in the $\sqrt{3} \times \sqrt{3}$ structure compared to the $2 \times 2$ case. In fact, the Kohn-Sham wave function at the conduction-band bottom state of the OR-$\sqrt{3} \times \sqrt{3}$ structure has amplitude at unprotruded Si atoms whereas the conduction-bottom state is highly localized

at the green protruded Si atoms in the $2 \times 2$ case (Fig. 5). The deviation of the conduction-band bottom state can be related to the short distance between the protruded atoms in the $\sqrt{3} \times \sqrt{3}$ case. The band gap reduction is caused by the dispersive conduction band induced by the interaction between the protruded atoms.

In summary, we have performed density-functional calculations to clarify atomic and electronic structures of freestanding bilayer silicene. After extensive structural exploration, we have obtained four $1 \times 1$, two $\sqrt{3} \times \sqrt{3}$, and four $2 \times 2$ dynamically stable structures free from imaginary phonon frequencies. We have found that the atomic protrusion is a principal structural characteristics which stabilizes bilayer silicene and induces optimum lateral periodicity. We have identified the most stable bilayer silicene as the hex-OR-$2 \times 2$ structure and revealed that this is a semiconductor with the energy gap of 1.3 eV using the hybrid functional.

[1] T. Ohta, A. Bostwick, T. Seyller, K. Horn, and E. Rotenberg, Science **313**, 951 (2006).

[2] E. McCann, Phys. Rev. B **74**, 161403 (2006).

[3] E. V. Castro, K. S. Novoselov, S. V. Morozov, N. M. R. Peres, J. M. B. Lopes dos Santos, J. Nilsson, F. Guinea, A. K. Geim, and A. H. Castro Neto, Phys. Rev. Lett. **99**, 216802 (2007).

[4] Y. Zhang, T.-T. Tang, C. Girit, Z. Hao, M. C. Martin, A. Zettl, M. F. Crommie, Y. R. Shen, and F. Wang, Nature (London) **459**, 820 (2009).

[5] A. Luican, G. Li, A. Reina, J. Kong, R. R. Nair, K. S. Novoselov, A. K. Geim, and E. Y. Andrei, Phys. Rev. Lett. **106**, 126802 (2011).

[6] K. Uchida, S. Furuya, J.-I. Iwata, and A. Oshiyama, Phys. Rev. B **90**, 155451 (2014).

[7] C.-C. Liu, W. Feng, and Y. Yao, Phys. Rev. Lett. **107**, 076802 (2011).

[8] M. Ezawa, Phys. Rev. Lett. **109**, 055502 (2012).

[9] M. Ezawa, Phys. Rev. Lett. **110**, 026603 (2013).

[10] P. Vogt, P. De Padova, C. Quaresima, J. Avila, E. Frantzeskakis, M. C. Asensio, A. Resta, B. Ealet, and G. Le Lay, Phys. Rev. Lett. **108**, 155501 (2012).

[11] C.-L. Lin, R. Arafune, K. Kawahara, N. Tsukahara, E. Minamitani, Y. Kim, N. Takagi, and M. Kawai, Appl. Phys. Exp. **5**, 045802 (2012).

[12] B. Feng, Z. Ding, S. Meng, Y. Yao, X. He, P. Cheng, L. Chen, and K. Wu, Nano Lett. **12**, 3507 (2012).

[13] D. Chiappe, C. Grazianetti, G. Tallarida, M. Fanciulli, and A. Molle, Adv. Mater. **24**, 5088 (2012).

[14] A. Fleurence, R. Friedlein, T. Ozaki, H. Kawai, Y. Wang, and Y. Yamada-Takamura, Phys. Rev. Lett. **108**, 245501 (2012).

[15] H. Jamgotchian, Y. Colignon, N. Hamzaoui, B. Ealet, J. Y. Hoarau, B. Aufray, and J. P. Bibérian, J. Phys.: Condens. Matter **24**, 172001 (2012).

[16] Z.-X. Guo, S. Furuya, J.-I. Iwata, and A. Oshiyama, J. Phys. Soc. Jpn. **82**, 063714 (2013).

[17] Z.-X. Guo, S. Furuya, J.-I. Iwata, and A. Oshiyama, Phys. Rev. B **87**, 235435 (2013).

[18] R. Arafune, C.-L. Lin, K. Kawahara, N. Tsukahara, E. Minamitani, Y. Kim, N. Takagi, and M. Kawai, Surf. Sci. **608**, 297 (2013).

[19] P. De Padova, P. Vogt, A. Resta, J. Avila, I. Razado-Colambo, C. Quaresima, C. Ottaviani, B. Olivieri, T. Bruhn, and T. Hirahara, Appl. Phys. Lett. **102**, 163106 (2013).

[20] A. Resta, T. Leoni, C. Barth, A. Ranguis, C. Becker, T. Bruhn, P. Vogt, and G. L. Lay, Sci. Rep. **3**, 2399 (2013).

[21] Z.-X. Guo and A. Oshiyama, Phys. Rev. B **89**, 155418 (2014).

[22] Z.-X. Guo and A. Oshiyama, New J. Phys. **17**, 045028 (2015).

[23] K. Takeda and K. Shiraishi, Phys. Rev. B **50**, 14916 (1994).

[24] S. Cahangirov, M. Topsakal, E. Aktürk, H. Şahin, and S. Ciraci, Phys. Rev. Lett. **102**, 236804 (2009).

[25] J. Bai, H. Tanaka, and X. C. Zeng, Nano Res. **3**, 694 (2010).

[26] T. Morishita, M. J. Spencer, S. P. Russo, I. K. Snook, and M. Mikami, Chem. Phys. Lett. **506**, 221 (2011).

[27] H. Fu, J. Zhang, Z. Ding, H. Li, and S. Meng, Appl. Phys. Lett. **104**, 131904 (2014).

[28] C. Lian and J. Ni, AIP Adv. **3**, 052102 (2013).

[29] W. Luo, Y. Ma, X. Gong, and H. Xiang, J. Am. Chem. Soc. **136**, 15992 (2014).

[30] B. Huang, H.-X. Deng, H. Lee, M. Yoon, B. G. Sumpter, F. Liu, S. C. Smith, and S.-H. Wei, Phys. Rev. X **4**, 021029 (2014).

[31] J. E. Padilha and R. B. Pontes, J. Phys. Chem. C **119**, 3818 (2015).

[32] K. C. Pandey, Phys. Rev. Lett. **47**, 1913 (1981).

[33] N. Troullier and J. L. Martins, Phys. Rev. B **43**, 1993 (1991).

[34] P. Giannozzi, S. Baroni, N. Bonini, M. Calandra, R. Car, C. Cavazzoni, D. Ceresoli, G. L. Chiarotti, M. Cococcioni, I. Dabo, A. Dal Corso, S. de Gironcoli, S. Fabris, G. Fratesi, R. Gebauer, U. Gerstmann, C. Gougoussis, A. Kokalj, M. Lazzeri, L. Martin-Samos, N. Marzari, F. Mauri, R. Mazzarello, S. Paolini, A. Pasquarello, L. Paulatto, C. Sbraccia, S. Scandolo, G. Sclauzero, A. P. Seitsonen, A. Smogunov, P. Umari, and R. M. Wentzcovitch, J. Phys.: Condens. Matter **21**, 395502 (2009).

[35] P. Hohenberg and W. Kohn, Phys. Rev. **136**, B864 (1964).

[36] W. Kohn and L. J. Sham, Phys. Rev. **140**, A1133 (1965).

[37] J. P. Perdew, K. Burke, and M. Ernzerhof, Phys. Rev. Lett. **77**, 3865 (1996).

[38] J. Heyd, G. E. Scuseria, and M. Ernzerhof, J. Chem. Phys. **118**, 8207 (2003).

[39] J. Heyd, G. E. Scuseria, and M. Ernzerhof, J. Chem. Phys. **124**, 219906 (2006).

[40] S. Baroni, P. Giannozzi, and A. Testa, Phys. Rev. Lett. **58**, 1861 (1987).

[41] X. Gonze, Phys. Rev. A **52**, 1096 (1995).

[42] S. Baroni, S. de Gironcoli, A. Dal Corso, and P. Giannozzi, Rev. Mod. Phys. **73**, 515 (2001).

[43] See Supplemental Material at http://link.aps.org/supplemental/10.1103/PhysRevB.91.201405 for details of computational method and structural exploration.

[44] A. Kokalj, Comput. Mater. Sci. **28**, 155 (2003).

[45] S. Cahangirov, V. O. Özçelik, L. Xian, J. Avila, S. Cho, M. C. Asensio, S. Ciraci, and A. Rubio, Phys. Rev. B **90**, 035448 (2014).